ATMOSPHERIC ENVIRONMENT: X 27 (2025) 100353

Contents lists available at ScienceDirect

Atmospheric Environment: X

journal homepage: www.journals.elsevier.com/atmospheric-environment-x

Reduced contrail radiative effect for fleets with low soot and water vapour emissions

Milenko Rubin-Zuzic [a,*], Luca Bugliaro [a], Andreas Marsing [a], Ziming Wang [a,b], Christiane Voigt [a,b], Christopher Simson [c], Sascha Kaiser [c], Paul Ziegler [c]

[a] Deutsches Zentrum für Luft- und Raumfahrt (DLR), Institut für Physik der Atmosphäre, Münchner Str. 20, Oberpfaffenhofen, 82234, Germany
[b] Johannes Gutenberg-Universität Mainz, Institut für Physik der Atmosphäre, Mainz, 55099, Germany
[c] MTU Aero Engines AG, Dachauer Str. 665, Munich, 80995, Germany

ARTICLE INFO

Keywords:
Contrails
Climate impact
WET engine
Soot
Water vapour

ABSTRACT

Besides the goal of net-zero carbon dioxide (CO_2) emissions, reducing aviation's climate impact also involves addressing other forcing effects, particularly radiative forcing from contrails. Current understanding suggests that decreasing both soot and water vapour emissions from aircraft engines reduces the occurrence and persistence of contrails, thereby lowering their radiative forcing. This may be achieved by engine concepts that combine water recovery from the exhaust with particle washout. This study presents an idealized sensitivity analysis using the Contrail Cirrus Prediction (CoCiP) model to assess how reductions in soot number and water vapour emissions could affect the radiative impact of contrail cirrus over Europe. The emission scenarios are not tied to any specific engine design but are chosen to explore the physical sensitivity of contrail formation and radiative effects. The number of emitted soot particles is reduced by up to two orders of magnitude, and water vapour emissions by one. We find that the mitigation effect becomes more pronounced with higher emission reductions. While both components contribute to the overall reduction, their combination leads to a stronger effect. The magnitude of the effect depends on their interactions during contrail formation and on subsequent atmospheric processes. The radiative forcing response exhibits marked geographic variability, with the strongest effects over regions with frequent ice-supersaturated air masses. Daily and seasonal variations in contrail occurrence and radiative impact further modulate the overall mitigation potential. The simulations indicate a substantial decrease in contrail radiative effect if technologies that lower soot and water vapour emissions are applied across a broad fleet. A limitation of this study is that other contrail nucleation pathways, such as condensation on volatile particles, are not considered. Thus, our assessment may provide an upper bound on the reduction of contrail cirrus radiative impact from soot and/or water vapour emissions.

1. Introduction

Aviation contributes to the anthropogenic effective radiative forcing (ERF) with a share of about 3.5% (Lee et al., 2021), including only the flight activities themselves. On the pathway to achieving the climate targets set by the Paris Agreement, aviation's non-CO_2 effects, including mainly contrails and NO_x emissions, must be considered alongside CO_2 reductions. This necessitates highly transformative technological and regulatory advancements in the predominantly fossil fuel-driven aviation sector. The mentioned radiative impact arises from a modification (forcing) of the atmosphere's solar and thermal radiation budget through substances injected from engine emissions. These instantaneous forcings drive the atmosphere out of equilibrium, the restoration of which leads to adjustments in the Earth's system or climate. ERF accounts for stratospheric and tropospheric adjustments, which reflect a part of the climate effect.

The main contributors to the net aviation ERF of 101 mW/m^2 in the year 2018 are CO_2 with an ERF of 34 mW/m^2, NO_x with 18 mW/m^2 and contrail cirrus clouds with 57 mW/m^2 with a 70% uncertainty range for the ERF of contrail cirrus clouds (Lee et al., 2021). Contrail cirrus form from water vapour in the exhaust and the atmosphere when the combustion process takes place in sufficiently cold and humid conditions in the presence of condensation nuclei, which at present mainly consist of soot from the engines. Both the absolute value and the uncertainty of the contrail cirrus ERF underline the importance of evaluating the impact of new engine concepts on contrails, considering the formation of contrail cirrus clouds as well as their life cycle and

* Corresponding author.
E-mail address: milenko.rubin-zuzic@dlr.de (M. Rubin-Zuzic).

https://doi.org/10.1016/j.aeaoa.2025.100353
Received 17 December 2024; Received in revised form 10 June 2025; Accepted 2 August 2025
Available online 11 August 2025

radiative impact. Contrail cirrus produces negative radiative forcing through the reflection of shortwave solar radiation during the day, as well as positive radiative forcing through the absorption and emission of longwave terrestrial radiation. The overall effect of contrail cirrus clouds is considered to result in positive radiative forcing (Lee et al., 2021; Schumann et al., 2015; Burkhardt and Kärcher, 2011). Mitigating the occurrence of contrails that cause positive radiative forcing provides a strong reduction potential to the aviation radiative impact, as the effect onsets immediately within a few hours, as compared to CO_2, which contributes to long-term climate forcing because of its multi-decadal lifetime and interactions within the global carbon cycle.

Among several innovative engine designs, the Water-Enhanced Turbofan (WET) concept offers a theoretical framework for substantial reduction of CO_2, NO_x, and contrail formation from aircraft (Kaiser et al., 2022), thereby providing a valuable perspective for more sustainable aviation. The concept promises to reduce contrail impact by recovering water from the exhaust, hence creating a drier exhaust, and by washing out particles. While this combination is technically attractive, other concepts may also achieve similar or even greater reductions. For example, hydrogen combustion eliminates CO_2 and soot emissions. When combined with optimized navigational contrail avoidance, it may also help reduce contrails. However, hydrogen exhaust contains significantly more water vapour than Jet-A, which could enhance contrail formation unless this is counteracted by specific mitigation strategies. Hybrid propulsion architectures and advanced fuel formulations may also contribute to multi-dimensional climate mitigation.

Hydrogen propulsion, whether based on combustion or fuel cell systems, is increasingly considered a long-term solution for reducing carbon emissions in aviation. While hydrogen eliminates soot and carbon dioxide emissions, it increases water vapour emissions, which can raise the likelihood of contrail formation and persistent ice supersaturation. Bier et al. (2024) show that contrails from hydrogen powered aircraft differ from conventional ones in terms of microphysical properties and optical characteristics. However, scientific understanding is still limited, mainly due to the lack of direct measurements and validated models for particle formation in hydrogen exhaust plumes.

To gain first insights into the contrail properties and radiative effects of low-soot, low-water vapour engines, we present a model-based analysis. For these investigations, we use the Contrail Cirrus Prediction Model (CoCiP, Schumann, 2012). This model simulates individual contrails using a Lagrangian approach, starting from routes and emissions of a given fleet and computing their radiative effect. CoCiP is a simplified and time-efficient model and has been compared to numerous contrail observations from existing engines. As a first step, we perform idealized sensitivity studies to investigate the impact of reduced exhaust particle emissions and water vapour on these quantities compared to a standard fleet of current aircraft.

The following sections briefly introduce the CoCiP model including the model setup, Section 3 reports on the results of the sensitivity studies, followed by a short description of the WET concept that is highlighted in this paper as an example of a concept leasing to low-soot and low-water vapour emissions. Lastly, a summary and outlook on subsequent activities is given.

2. Contrail Cirrus Prediction model CoCiP

2.1. General CoCiP description

The Contrail Cirrus Prediction (CoCiP) model (Schumann, 2012; Schumann et al., 2021b) is used to simulate contrail properties (see end of Section 2.6) and their associated instantaneous radiative forcing for aircraft powered by kerosene-burning turbofan and turboprop engines. These simulations can be conducted for individual flights or entire fleets over seasonal and annual timescales, using only a small number of input parameters derived from meteorological and engine data, combined with a simplified representation of the underlying physical processes.

CoCiP has been evaluated in several studies, showing good agreement with both observational data and other modelling approaches. For instance, Schumann and Heymsfield (2017) demonstrated that the model's predictions of ice water content, ice crystal number concentrations, and optical properties match well with in-situ and satellite observations, as well as with results from other contrail models. Schumann and Graf (2013) validated the model's ability to reproduce patterns of contrail coverage and radiative forcing over the North Atlantic. Furthermore, Schumann et al. (2021b) compared CoCiP output during six months of the COVID-19 pandemic with satellite measurements of optical properties and top-of-atmosphere radiation, again finding reasonably good consistency.

The model integrates several key components in its simulation of contrail formation and evolution. It considers numerical weather prediction data (Section 2.4), to assess regional or global meteorological conditions. This meteorological data is crucial for simulating the environment in which aircraft operate. The model then simulates contrails for individual aircraft flights, incorporating specific flight data such as waypoints, aircraft types, and engine properties, to generate accurate representations of flight paths, aircraft characteristics and operational state. Aircraft properties are obtained from the Base of Aircraft Data (BADA3) data set from EUROCONTROL. In determining where and if contrails form, CoCiP employs the Schmidt-Appleman criterion (SAC Appleman, 1953; Schumann, 1996), which sets a threshold for the formation of contrails at a given atmospheric temperature and humidity. The SAC follows the mixing of hot and humid exhaust gases with the ambient atmosphere and is fulfilled if saturation with respect to liquid water is reached during dilution, at which point droplets form on condensation nuclei. After freezing, the crystals only persist (grow, not sublimate) if the atmosphere is supersaturated with respect to ice.

Additionally, the model considers the impact of aircraft wake vortices, which substantially influence the formation and initial dispersion of contrails. These vortices can alter the distribution and density of contrails in the immediate aftermath of their formation. Once a contrail forms, CoCiP estimates its initial properties, such as the mass and number concentrations of ice crystals. This estimation is vital for understanding the physical characteristics of the contrail from its inception. CoCiP employs a Lagrangian Gaussian plume model to track the advection and evolution of contrail segments emerging from the flight paths, from formation to dissipation or evaporation, considering mixing and bulk cloud processes through a combination of quasi-analytical methods and an effective numerical scheme. This temporal analysis is crucial for understanding the life cycle of contrails and their potential environmental impacts.

CoCiP treats ice nucleation, wake vortex dynamics and ice microphysics in a simplified and computationally efficient way by utilizing streamlined algorithms that approximate these complex processes without the need for extensive computational resources. This approach, while less detailed than the comprehensive simulations in more advanced models (e.g., Bier and Burkhardt, 2022; Verma and Burkhardt, 2022), still provides valuable insights into contrail formation and evolution.

In addition, CoCiP does not include feedback mechanisms on meteorological input parameters, i.e. it does not incorporate interactive feedbacks between contrails and the surrounding atmosphere (as done in part e.g. in Schumann et al., 2015). For example, contrail-induced changes in local temperature, humidity, and large-scale ice cloud coverage are not dynamically modelled. Previous studies have shown that such interactions (e.g., subsidence effects and modifications of ice supersaturation) can considerably influence contrail evolution and radiative forcing (Burkhardt et al., 2018).

CoCiP predicts various contrail-related characteristics for each waypoint of each flight, as well as the distribution of some contrail parameters over the considered region in hourly intervals. Per hour,

Table 1
Four key two-dimensional fields predicted by CoCiP are presented which characterize contrail radiative effects (RFnet, RFSW, RFLW) and contrail optical thickness (TAUCO) over the European domain. These fields represent instantaneous snapshots taken at fixed hourly intervals rather than time-averaged values.

Variable	Unit	Description
RFLW	W/m^2	Instantaneous longwave radiative forcing by contrails and contrail cirrus
RFSW	W/m^2	Instantaneous shortwave radiative forcing by contrails and contrail cirrus
RFnet	W/m^2	Net instantaneous radiative forcing by contrails and contrail cirrus, RFnet=RFLW+RFSW
TAUCO		Optical thickness of contrails and contrail cirrus

we consider four quantities that are predicted over the entire domain (see Table 1).

The net instantaneous radiative forcing (RFnet) quantifies the combined effect of contrails on solar (shortwave, RFSW) and terrestrial (longwave, RFLW) radiation at the top of the Earth's atmosphere. Contrails with negative RF (cooling contrails) can only occur during daytime under specific atmospheric and surface condition, when the shortwave reflection of sunlight exceeds the absorption from trapped infrared radiation. At night RFSW vanishes, therefore RFnet = RFLW > 0 W m^{-2} and only warming contrails can be observed. RFSW dominates over RFLW at small solar zenith angles, for higher contrail optical thickness, and over dark and cold surfaces, such as cloud-free ocean regions (Schumann, 2012; Meerkötter et al., 1999) while contrails over bright and warm surfaces (e.g., snow-covered land or optically thick clouds) tend to cause net warming. However, the occurrence of cooling contrails is limited, and their overall contribution is small compared to the dominant longwave-driven warming effect in the annual mean (see e.g. Fig. 5).

Teoh et al. (2022a) have shown (for ERA5) that relative humidity corrections affect the CoCiP results in a relevant way. The correction method used in this study adjusts relative humidity over ice RHi such that the statistical distribution of upper-tropospheric relative humidity better matches in-situ observations from the IAGOS dataset. More advanced calibration methods for ambient relative humidity, including deep neural networks and histogram matching against satellite retrievals (Wang et al., 2025; Platt et al., 2024; Wolf et al., 2025) are also becoming available, but are not integrated in this study. Our contrail predictions address the critical aspect of UT RHi uncertainty in NWP models but are of course dependent on the bias correction approach selected.

Please notice that in the following we do not distinguish between contrails and contrail cirrus and all the quantities in Table 1 refer to both of them. When we talk about the contrail radiative forcing of contrails we always mean the (instantaneous) radiative forcing of contrails and contrail cirrus.

2.2. Ice nucleation in CoCiP

CoCiP considers nucleations on emitted soot particles. In conventional turbines, during combustion of kerosene, on average about 10^{15} soot particles are emitted per kilogram fuel burned. The soot particles in the exhaust plume, or at least a fraction of them (Unterstrasser and Gierens, 2010; Unterstrasser, 2014, 2016), initiate the formation of liquid droplets that freeze to ice crystals which then can grow and produce contrails depending on other atmospheric conditions, like humidity, temperature, wind and further parameters. Engine non-volatile particle emissions, or more precisely soot emission indices, for conventional engines are computed with a method that scales International Civil Aviation Organization (ICAO) emission data according to the given thrust load (Teoh et al., 2022a). This so-called T4/T2 methodology involves the calculation of the ratio between the combustor exit temperature (T4) and the engine inlet temperature (T2) to estimate the non volatile particle matter (nvPM) emissions. A constant soot number emission index of 10^{15} soot particles emitted per kilogram of fuel burned is assumed when specific engine data are not available. The size of the soot particles emitted also influences contrail properties (Yu et al., 2024), but is not considered in CoCiP.

A precise knowledge of the emitted nvPM number is important because for conventional fuel they act as the main source of ice nucleation (Kleine et al., 2018). However, in addition to soot particles (black carbon aggregates, Petzold et al., 1999) the engine exhaust plumes contain also entrained ambient aerosol particles, ultrafine liquid volatile particles (Yu et al., 1999) and possibly lubrication oil droplets (Ungeheuer et al., 2022). Natural background aerosol is expected to play a role in ice particle formation in the soot-poor regime with soot concentrations of 10^{12}–10^{13} particles per kilogram of fuel burned or lower (Kärcher and Yu, 2009) and to play a major role in contrail formation from hydrogen combustion (Bier et al., 2024). Volatile particles (vPM) stem from condensable vapours in the aircraft plume formed during cooling and consist of both inorganic (sulfates formed by the oxidation of sulfur in the fuel, Kärcher and Fahey, 1997; Timko et al., 2010) and organic material (unburned fuel and aircraft lubrication oil, Ungeheuer et al., 2022). This vPM is important not only because it can condense upon soot, modifying its properties (Kärcher and Fahey, 1997; Schumann et al., 1996), but also because it can nucleate new particles (Yu et al., 1999; Timko et al., 2010; Ponsonby et al., 2024). This alternative nucleation pathway can become important when fuel sulfur content is large enough (Schumann et al., 1996) or soot emissions are very low (in the range of $<10^{13}$–10^{14} particles per kg fuel) (Kärcher and Yu, 2009; Kärcher, 2018; Yu et al., 2024).

The ice nucleation scheme in CoCiP (Schumann, 2012) was evaluated using in-situ contrail measurements from engines burning conventional Jet-A fuel, typically producing soot number emissions of 10^{14} to 10^{15} particles per kg fuel (Schumann and Graf, 2013). These parameterizations may not fully capture the microphysics of exhaust plumes from alternative technologies with significantly lower soot concentrations or different particle characteristics as e.g. an altered soot particle size distribution. In the absence of observational data for such configurations, we apply the scheme under the assumption that only soot number concentration varies, while other particle properties remain unchanged.

Since CoCiP does not explicitly account for these additional nucleation processes, it may overestimate the potential for contrail suppression in very low-soot scenarios. Additionally, engine-emission scaling methods, such as the T4/T2 approach, can sometimes produce unrealistically low soot emissions when applied outside their calibrated range. To prevent artificial suppression of contrails in cases where alternative nucleation pathways might still enable their formation, we enforce a 10^{13} kg^{-1} threshold as a practical boundary beyond which further microphysical refinements are needed and aligns with practices in other studies (e.g. Teoh et al., 2022a). Maintaining this constraint ensures that the model remains within empirically observed emission ranges. However, this lower limit introduces uncertainties when applied to very low-soot engine concepts, where alternative nucleation pathways

may become relevant. As a result, the expected reduction in contrail radiative forcing presented in Sections 3.2 and 3.4 may be partially offset in scenarios of extreme soot emission reductions. Therefore, our results should be interpreted as an upper-bound estimate of the maximum potential mitigation in contrail cirrus climate impact. The volatile particle activation and entrained aerosols in ice nucleation (Yu et al., 2024; Dischl et al., 2024; Bier et al., 2024; Ungeheuer et al., 2022; Ponsonby et al., 2024) are beyond the scope of this study. Future experimental work should assess, under real-world conditions, which properties contrails have that form at low-soot conditions and the role of alternative aerosol species, refining mitigation estimates for next-generation low-emission aviation technologies.

2.3. Geographic domain

For our analysis of the low-soot and low-water vapour effects on contrails, we examine flight traffic data from 2019, which represents the last year before the onset of the COVID pandemic and thus provides a benchmark for normal (high) traffic conditions.

Our investigation is limited to the geographical region between 20° W and 20° E longitude, and 35° N to 60° N latitude, covering a substantial portion of the European continent (see Fig. 1). The area spans a wide range of latitudes and includes various geographical features such as mountains, plains, and coastlines. This diversity causes a wide range of weather conditions. The specified domain is of particular interest in aviation due to its high traffic volume. It is characterized by high traffic density, both in terms of passenger numbers and flight movements. The small geographic size of the continent relative to the volume of flights leads to one of the densest air traffic environments in the world. In 2019, the European region was a strong contributor to global air traffic. More than 800 million passengers were served by approximately 9.25 million flights at EU27 (European Union consisting of 27 member states) together with EFTA (European Free Trade Association) airports (EASA, 2022; IATA, 2025). Europe accounted for approximately 25% of the world's air traffic.

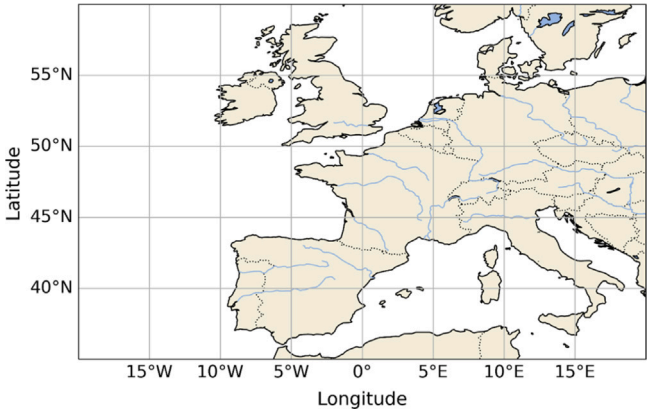

Fig. 1. Considered European air traffic domain.

2.4. Weather data

CoCiP uses numerical weather prediction (NWP) forecasts from the Integrated Forecasting System (IFS) model at ECMWF to simulate the impact of weather conditions on contrail formation and evolution. The horizontal resolution of this NWP data used for CoCiP is 0.25° (27.8 km at equator, 13.91 km at 60° and 22.8 km at 35° → average 18.8 km at 47.5° latitude). The IFS model uses a hybrid vertical coordinate system with 137 vertical levels (ECMWF Model Level Definitions, 2024). At cruising altitude between 33,000 and 42,000 feet this corresponds approximately to 300 m in vertical level distance. Quantities used are in particular temperature, horizontal and vertical wind, and humidity as a function of altitude. Temperature and humidity are particularly important since they control whether contrails are formed or not according to the SAC, and for contrail persistence: only contrails formed in supersaturated regions (with respect to ice) can grow, live for hours and extend to contrail cirrus (Gierens et al., 2020). These contrails are responsible for the largest fraction of contrail cirrus radiative forcing (Burkhardt et al., 2018; Kärcher, 2018; Burkhardt and Kärcher, 2011). However, humidity in cruise altitudes is most difficult to simulate by numerical weather prediction models (see Gierens et al., 2020; Dischl et al., 2022) and it is thus corrected to achieve a better agreement with in situ measurements (Teoh et al., 2022a; Schumann and Heymsfield, 2017; Wang et al., 2025). Here we use the approach of Teoh et al. (2022a):

$$RHi_{\text{corrected}} = \begin{cases} \frac{RHi}{a^l}, & \text{when } \frac{RHi}{a} \leq 1 \\ \min\left(\left(\frac{RHi}{a}\right)^b, 1.67\right), & \text{when } \frac{RHi}{a} > 1 \end{cases}$$

The original fit parameters $a = 0.9779$ and $b = 1.635$ are obtained by fitting ECMWF reanalysis ERA5 HRES data to IAGOS observations (Teoh et al., 2022a). CoCiP uses integrated forecast data, for which the parameters are modified to $a = 0.95$ and $b = 1.4$.

Contrail properties are highly sensitive to ambient humidity at cruise altitudes (Gierens et al., 2020). Even minor biases in the relative humidity over ice within the ECMWF forecast or reanalysis data can strongly affect the frequency and spatial extent of supersaturated air. This, in turn, influences both the occurrence and persistence of contrails, leading to potential over- or underestimations in contrail radiative forcing. Although we apply corrected humidity fields to mitigate such biases, uncertainties remain, particularly in regions with limited in situ measurements or strong vertical and horizontal humidity gradients.

2.5. Flight traffic

CoCiP uses traffic data for 2019 (see Fig. 2) from EUROCONTROL and the UK air navigation service provider NATS to simulate contrails in a large part of Europe and the Shanwick Oceanic Control Area above a flight level (FL) 180 (18,000 feet, about 5.5 km) (Schumann et al., 2021a).

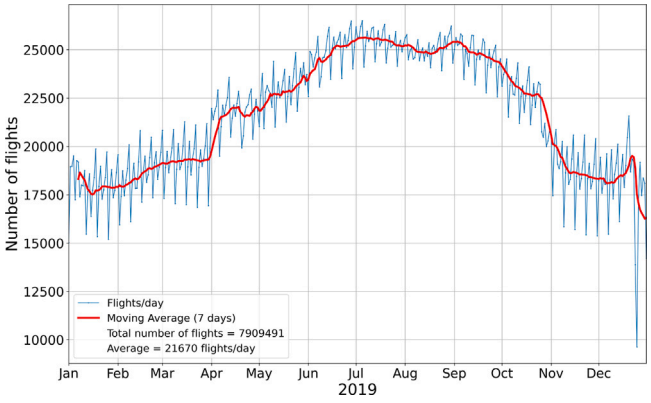

Fig. 2. Considered air traffic in 2019, with weekly peaks towards weekends and increased traffic during spring and summer due to tourism. Flight activity reaches its absolute minimum on 25th December. The red curve represents the moving average over 7 days.

To effectively model and analyse each flight, specific data inputs are required, including the aircraft type identified by its ICAO designator code, the ICAO airport codes for both departure and destination, an accurate estimate of the take-off mass, as well as the departure and arrival times. Additionally, a comprehensive sequence of waypoints detailing time, longitude, latitude, and flight level from the start to the end of the flight is essential. The data for flight routes is interpolated to maintain a consistent time increment of 60 s.

2.6. CoCiP sensitivity studies

Reducing the emission number of soot particles leads to a decrease in the number of ice particles in contrails, resulting in thinner and shorter-lasting contrails. This, in turn, leads to a smaller radiative forcing (Bier and Burkhardt, 2022; Burkhardt et al., 2018; Märkl et al., 2024). Reducing water vapour emissions leads to a notable decrease in specific humidity in the aircraft's wake. This should reduce the occurrence of contrail formation according to the SAC as well as the size, number, and optical thickness of the ice crystals formed affecting the contrails' radiative forcing and potentially their lifetime. In fact, the mixing line slope G (Schumann, 1996) in the SAC amounts to

$$G = \frac{c_p p_a}{\epsilon} \frac{EI_{H_2O}}{(1-\eta)Q} \quad (1)$$

where p_a is the ambient pressure in Pa, EI_{H_2O} the emission index of water vapour in kg/kg(fuel), η the overall propulsion system efficiency, Q = 43.6MJ/kg the heating value of kerosene, c_p = 1004 J/kg/K the isobaric heat capacity of air, and $\epsilon = 0.622$ the molar mass ratio of water vapour and dry air. The parameter G defines the maximum temperature T_{max} at which contrails can form (Schumann, 1996):

$$T_{max} = 226.69 + 9.43 \ln(G - 0.053) + 0.72 (\ln(G - 0.053))^2 \quad (2)$$

for $G \leq 2$ Pa/K. This temperature thresholds decreases when G decreases. For a "traditional" aircraft flying at 250 hPa with an overall propulsion efficiency of 0.4 and burning kerosene (with an EI_{H_2O} = 1.25 kg/kg(fuel)), G amounts to 1.93 Pa/K and T_{max}=233 K. With a reduction in water vapour emissions by one order of magnitude, G reduces to 0.193 Pa/K and T_{max}=211 K. See also Megill and Grewe (2025) for a more general discussion of G in the context of various future technologies.

For the sensitivity studies, first a reference simulation (baseline scenario) with the parameters given above for meteorology, air traffic, engine and fuel properties are performed. For the geographical and temporal simulation domain selected in this study (Europe, 2019, see Sections 2.3 and 2.5) the mean nvPM emission number computed with the T4/T2 procedure amounts to 1.56×10^{15}/kg and a small fraction of 4% of the computed nvPM data is smaller than 10^{13}/kg and is thus increased to 10^{13}/kg (Section 2.2). To account for the possible mitigation effects from low-soot technologies, we conduct sensitivity studies reducing soot emissions by 50%, one order of magnitude (90%), and two orders of magnitude (99%). In the most extreme case of 99% soot emission reduction, approx. 21% of the nvPM numbers fall below the lower threshold 10^{13}/kg and are thus replaced by 10^{13}/kg. This leads to a mean nvPM number of 1.67×10^{13}/kg in this situation instead of the 1.56×10^{13}/kg that were expected without this correction. Furthermore, for each soot reduction scenario we reduce water vapour emissions by 50% and 90% (see also the Supplementary Material). Finally, we compare simulations that include soot and/or water vapour reductions with the reference scenario without any emission reductions. The test grid in the two relevant parameters is visualized in Fig. 3 and results in 12 distinct CoCiP simulations, each producing four hourly parameters predicted over the entire domain during the full 2019 year (see Table 1).

These emission scenarios span a wide range of hypothetical combinations of soot and water vapour reductions, allowing a systematic analysis of their individual and combined impacts on contrail radiative properties. The grid was constructed to explore the effects of soot and water vapour reductions both separately and in combination in order to understand the model's results across a broader range of configurations. Our aim is not to replicate specific propulsion designs, but to evaluate the physical response of contrail properties under a wide range of emission profiles. The simulations modify only the emissions disregarding any change in combustion or fuel properties. For instance, no overall increase in efficiency is modelled in the current study.

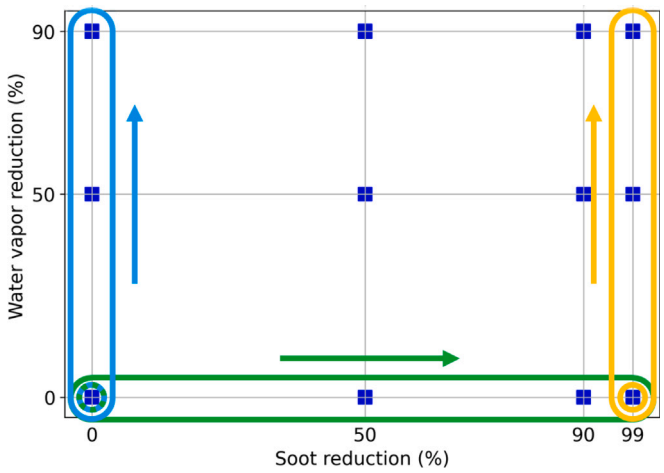

Fig. 3. Test grid of CoCiP model sensitivity studies exploring the soot and water vapour emission reductions and combined effects. Each blue marker corresponds to a separate simulation scenario, with soot reductions from 0% to 99% and water vapour reductions from 0% to 90%. The coloured circles around the blue markers for soot reduction of 0% and 99% at left and right bottom highlight the emissions of the different baseline scenarios (see Figs. 7, 8 and 9). Note that the grid was symmetrically defined in both dimensions to systematically explore the parameter space.

3. Results

For each CoCiP simulation run, we compute various statistical characteristics of the predicted variables (see Table 1) over the entire year 2019 for the considered European domain. The corresponding results are listed in Table 2 (see Section 3.4), which presents the mean and standard deviation of RFnet for all simulations, along with the percentage reduction relative to the baseline scenario without emission reductions. The primary advantage of this approach of averaging contrail impact data over a whole year is to provide an understanding of the overall contrail radiative effect. In general there is a substantial variation in contrail formation conditions, air traffic patterns, and meteorological conditions across different seasons. Averaging over these periods mitigates the effects of short-term variability in weather conditions (notably temperature and humidity) and air traffic, which can strongly influence contrail formation and their climate effects. The method ensures that the analysis captures the broad range of conditions under which contrails form and persist, providing a more reliable estimate of their overall average radiative effect. Nevertheless, year to year variability of atmospheric conditions and thus contrail radiative effects cannot be considered.

Since, as stated above, variability of contrail properties and contrail radiative effects (RFLW, RFSW, RFnet, TAUCO, see also Table 1) is very large, we first analyse an extreme event in Section 3.1 and the variability of hourly values of these quantities over the entire year 2019 together with the diurnal variability of RFnet.

To investigate the mean relative contrail changes for the year 2019 resulting from reductions in soot and water vapour emissions, the variation of these four important CoCiP output quantities are visualized relative to our baseline scenario when soot emissions are reduced (Section 3.2), when water vapour is reduced (Section 3.3) and when both soot and water vapour emissions are reduced (Section 3.4).

3.1. Variability of net radiative forcing

The effect of contrails and contrail cirrus on radiation, as well as their optical thickness, varies strongly from hour to hour and from day to day. Thus, to better understand this variability and to better characterize our simulations, we discuss four different aspects in this section. First, we illustrate a specific case where the contrail-induced

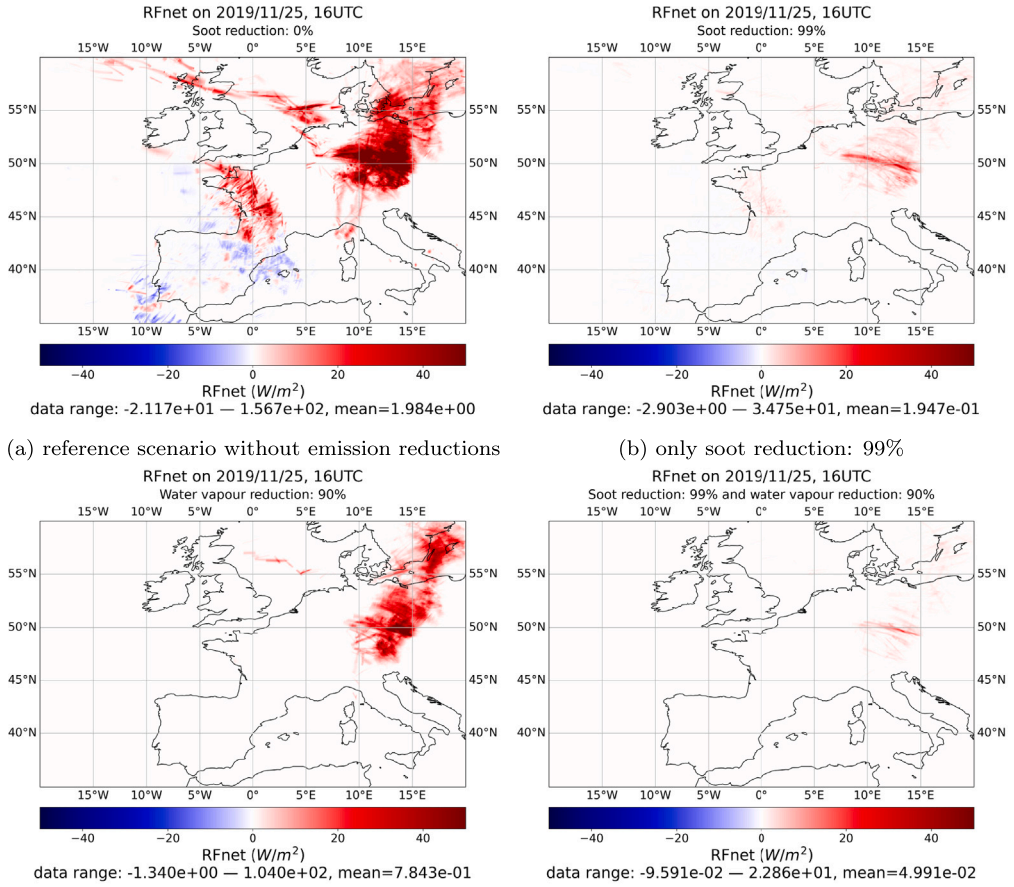

(a) reference scenario without emission reductions

(b) only soot reduction: 99%

(c) only water vapour reduction: 90%

(d) soot reduction: 99% and water vapour reduction: 90%

Fig. 4. Distribution of net instantaneous radiative forcing over Europe for different soot and water vapour emission reductions on 2019/11/25 at 16:00 UTC.

RFnet is particularly large at a given day and time, and discuss its spatial distribution over Europe. Of course, this situation does not represent a climatological average but rather an extreme scenario chosen to demonstrate particularly strong effects. Second, we contextualize this extreme event by showing the distribution of RFnet values over the entire year. Third, we discuss the diurnal cycle of RFnet over the entire domain to characterize RFnet as a function of the time of day, and in particular to observe the occurrence of positive and negative RFnet values. Finally, the Supplementary Material (Figures 1s and 2s) provides mean spatial distributions of RFnet over the full year 2019 for all sensitivity scenarios. These four aspects are intended to help understand the spatial and temporal distribution of RFnet, which is described in the following sections only as a mean annual value over the entire domain.

First of all we focus on November 25, 2019 at 16 UTC to the baseline scenario without soot and water vapour reduction (see Fig. 4a). At this specific time step the contrail-induced instantaneous net radiative forcing (RFnet) shows pronounced spatial variability over Europe. CoCiP computes substantial positive RFnet (indicated by red colours) with a mean value of nearly 2 W/m^2 which is approximately 10 times as large as the annual mean of 0.214 W/m^2. However, this does not represent a climatological average but rather an exceptional case selected to illustrate the strongest effects that occur.

Strong warming areas over Eastern Europe are simulated, stretching over a broad latitude and longitude domain. Similarly, in western France, we observe warming due to persistent contrails. There are also some regions of cooling contrails (blue colours), over north-east and south-west of Spain and the Biscay region, where distinct line-shaped structures corresponding to flight tracks are clearly visible. In Eastern Europe, the contrail impact is more extended and considerably higher, exceeding 100 W/m^2, which is much higher than the annual mean of 214 mW/m^2. With a 99% reduction in soot emissions (Fig. 4b), the overall impact of contrails strongly decreases. The maximum RFnet only reaches 35 W/m^2, the mean RFnet drops down to 0.195 W/m^2 (10% of results in Fig. 4a). Interestingly, the same regions where warming is observed before the soot reduction, are showing the same effect after soot reduction, indicating that the geographical patterns of contrail effects remain consistent despite changes in emission levels since they are dominated by the shape of the ice supersaturated regions. Cooling regions still occur, but are less pronounced and not visible when using the same colour scale.

When instead of soot the water vapour emission is reduced by 90% the decrease of RFnet is much smaller (Fig. 4c). The mean reaches 0.78 W/m^2 (40% of results in Fig. 4a). In the scenario with a simultaneous reduction by 99% in soot and 90% in water vapour emissions, the mean RFnet drops to 0.05 W/m^2, 2.5% when compared to the unreduced case (see Fig. 4d).

To complement the spatial snapshot shown in Fig. 4a, which illustrates an extreme instantaneous RFnet value at a single time step, Fig. 5 displays the diurnal and seasonal variability of contrail cirrus net radiative forcing over Europe. It reveals the temporal structure of contrail impacts throughout the year by showing the hourly mean RFnet for each day, based on CoCiP simulations for the baseline scenario (i.e., without reductions in soot or water vapour emissions). This comprehensive view captures characteristic temporal patterns in the radiative effects of contrails across the annual cycle.

Fig. 5 reveals that RFnet varies systematically with both time of day and season. During the early morning hours, RFnet tends to be

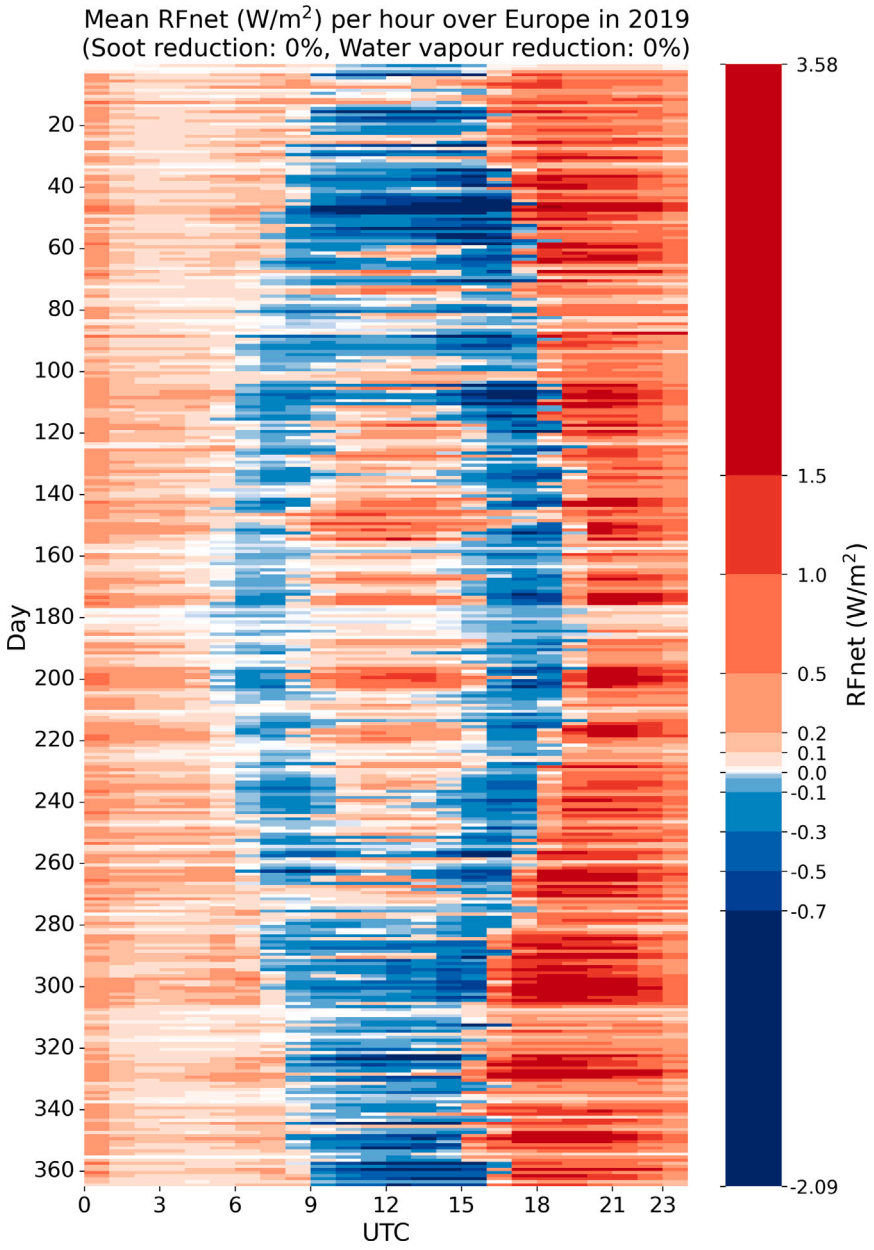

Fig. 5. Annual cycle of contrail cirrus net radiative forcing (RFnet) over Europe in 2019, based on hourly CoCiP predictions for the baseline scenario (soot reduction = water vapour reduction = 0%). RFnet is shown as a function of time of day (UTC, x-axis) and day of year (y-axis). The colour bar indicates the hourly mean RFnet in W m^{-2}, where red shades represent net warming and blue shades represent net cooling. The maximum and minimum RFnet values occurring throughout the year are shown at the top and bottom of the colour bar, respectively. The corresponding annual mean is 0.214 W m^{-2}; the standard deviation is given in Table 2.

lower than in the late evening, suggesting reduced longwave warming due to cooler and drier atmospheric conditions and/or dissipating contrails. At midday in summer, contrails predominantly produce net warming, while before and after noon, shortwave reflection becomes more effective and leads to localized net cooling. Notably, in spring and autumn, contrails induce net cooling even at midday, highlighting the importance of solar zenith angle and surface albedo in modulating the radiative response. Throughout the nighttime hours, RFnet remains positive, consistent with the absence of shortwave forcing. These findings complement the spatial patterns in Fig. 4d by illustrating how temporal factors, not just geography or flight activity, shape the radiative impact of contrails. The appearance of cooling contrails is restricted to specific windows of time, especially during clear-sky conditions in the transitional seasons, whereas net warming dominates on average.

To further characterize the statistical structure of net radiative forcing and complement the spatially averaged data presented in Table 2, we examine the temporal evolution of domain-averaged RFnet in 2019. For each hour, the spatial mean RFnet across the entire European domain is calculated using the baseline scenario without emission reductions. The resulting time series is then used to construct the frequency distribution shown in Fig. 6. Each data point in this histogram represents the mean RFnet over Europe at a given hour. This approach complements the diurnal structure shown in Fig. 5 and is different from the analysis in Table 2 and Figs. 7–9, where the statistics are based on the annual mean RFnet at each grid point, followed by computation of spatial variability. In those cases, the standard deviation quantifies spatial heterogeneity in the annual mean field. In contrast, the distribution in Fig. 6 captures the temporal variability of domain-wide RFnet on an hourly basis. The histogram in Fig. 6

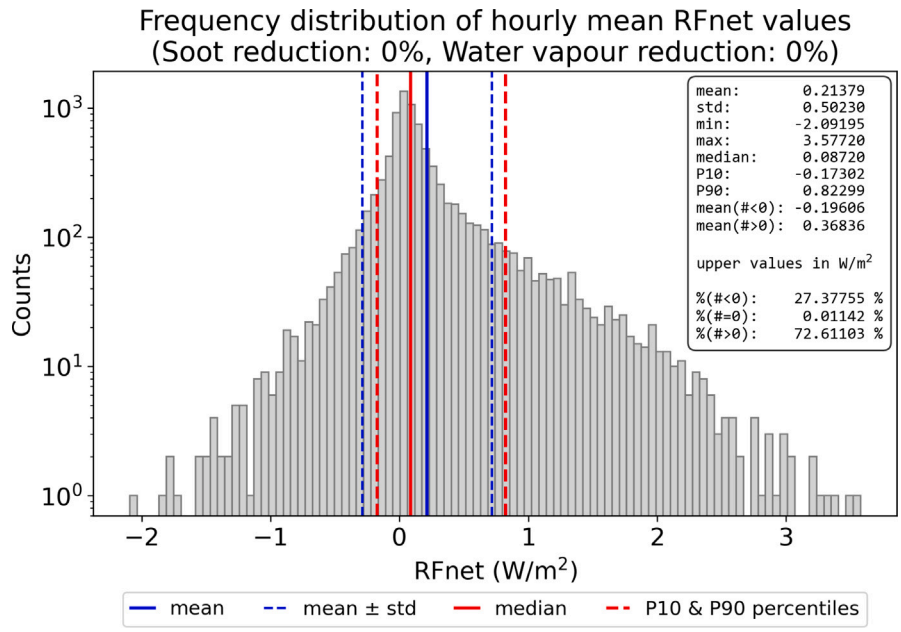

Fig. 6. Histogram of domain-averaged hourly RFnet values for the year 2019 (baseline case with 0% soot and water vapour reduction). The logarithmic frequency distribution highlights the asymmetry and intermittency of contrail radiative forcing. Indicated are the mean and median values, standard deviation, 10th and 90th percentiles, as well as the relative frequency and average strength of negative, zero, and positive RFnet hours.

reveals a strongly right-skewed distribution: the majority of hourly values cluster near zero, while a smaller number of extreme cases reach domain-mean RFnet values up to 3.6 W m^{-2}. The mean over all hourly values is 0.214 W m^{-2}, identical to the mean derived from the spatially averaged annual map. However, the standard deviation in this case is 0.50 W m^{-2}, reflecting the intermittent and episodic nature of contrail radiative forcing. This value cannot be directly compared to the standard deviations in Table 2, as it arises from temporal rather than spatial variation. The distribution also quantifies the relative occurrence of cooling and warming events. About 27.4% of the hours show negative domain-averaged RFnet, with a mean of approximately −0.20 W m^{-2}, indicating that temporary net cooling from contrail cirrus is a recurring feature, albeit generally of smaller magnitude. In contrast, 72.6% of the hours exhibit positive RFnet, with a higher mean of +0.37 W m^{-2}, reflecting the dominance of longwave warming in contrail radiative forcing. Only a negligible fraction of hours (~0.01%) show values at exactly zero, indicating that no contrails were present in the model domain during those times. By comparing this temporal distribution with the spatially resolved patterns in the main figures, we demonstrate that mitigation strategies must consider both when and where contrail formation is most effective, and that emission reductions targeting these peak periods and locations could yield the greatest climate benefit.

While Fig. 5 reveals systematic diurnal and seasonal patterns in the hourly RFnet evolution, the histogram in Fig. 6 highlights the statistical intermittency and asymmetry underlying these patterns. Together, they illustrate both the structured and stochastic components of contrail radiative forcing throughout the year.

3.2. Reduction of soot particle emission

In this section we investigate the change in the mean values of RFLW, RFSW, RFnet and TAUCO (Table 1) over the full year 2019 with respect to our baseline scenario (0% soot reduction, 0% water vapour reduction) in Fig. 7 when soot emissions are reduced. The vertical axes indicate the percentage change of the simulated quantities relative to their corresponding baseline scenario (point (0,0)), while the horizontal axis represents the percentage reduction in soot.

When the soot emission is reduced (see Fig. 3 with CoCiP runs marked in green) in terms of number (and implicitly in terms of mass), the contrail related variables decrease monotonically and non-linearly (Fig. 7). Their slope increases towards higher soot emission reduction. At 50% soot reduction RFnet is decreased by 20% and TAUCO is decreased by 27% indicating fewer and optically thinner contrails. For a soot reduction of 99%, RFnet decreases by 88% and TAUCO by 92%. This suggests a substantial annual decrease in the warming effect attributed to contrails if all aircraft reduced their soot particle emissions by two orders of magnitude. Soot particles primarily act as condensation nuclei for droplets that later form contrail ice particles. Reducing the number of ice particles while maintaining their bulk mass leads to bigger crystals. These have a reduced optical thickness in the solar spectrum due to less scattering, but more importantly they sediment faster. As soon as they leave the ice-supersaturated region, they start to sublimate in lower and thus warmer regions, reducing contrail lifetime and radiative effect.

The effect of reduced ice crystal numbers on the (stratospherically adjusted) radiative forcing of contrails has been calculated by Burkhardt et al. (2018) using a global climate model for an air traffic inventory in 2006. They find that a reduction in initial ice crystal numbers by 90% leads to a reduction in radiative forcing by 69%, while reducing the initial ice crystal numbers by 50% leads to a reduction in radiative forcing by 21%. Bier and Burkhardt (2022) use an improved global model version to calculate the effect of a soot particle reduction on the radiative forcing of contrails and they show similar trends compared to their 2018 results: a reduction in soot emissions by 50% and 90% leads to a reduction in radiative forcing by 15 and 59%. The relative reduction in the radiative forcing from contrails calculated by Burkhardt et al. (2018) and by Bier and Burkhardt (2022) for a 50% and a 90% reduction in soot particle emissions with the global climate model for the air traffic inventory in 2006 is thus comparable to the reduction of contrail radiative effect calculated with the CoCiP contrail model (20% and 60%) for air traffic and weather in Europe in 2019. The relative reduction in contrail optical properties and radiative effect is also in line with results from Teoh et al. (2022b, 2024), who calculated the effects of SAF blending on particle emissions, contrails and the contrail RFnet.

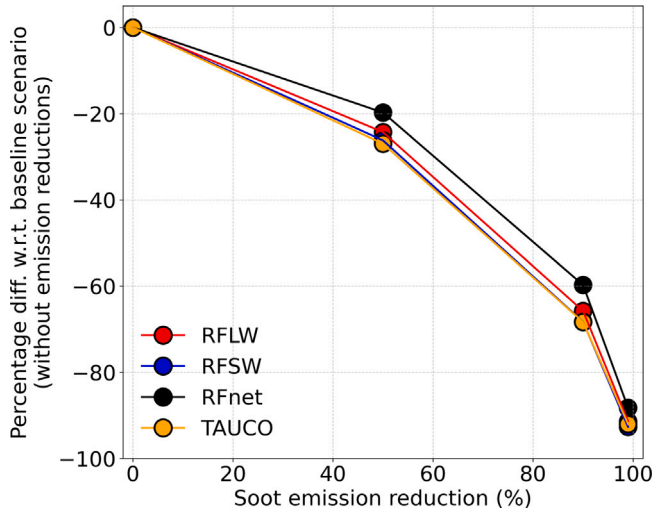

Fig. 7. Percentage difference of RFnet, RFSW, RFLW and TAUCO (see Table 1) w.r.t. baseline scenario (0% soot reduction, 0% water vapour reduction) vs. soot emission reduction in % (mean results for 2019).

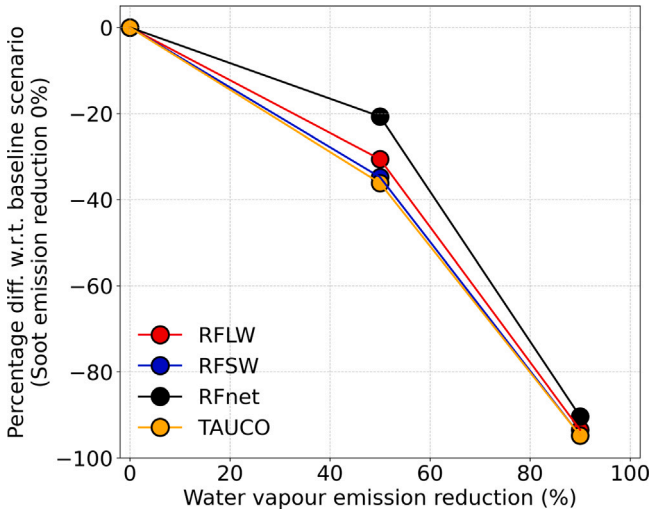

Fig. 8. Percentage difference of RFnet, RFSW, RFLW and TAUCO (see Table 1) w.r.t. baseline scenario (0% soot reduction, 0% water vapour reduction) vs. water vapour emission reduction (mean results for 2019).

Reductions in soot particle number by up to 90% are supported by current developments in low-emission combustor technologies such as TAPS and RQL (Burkhardt et al., 2018). Even stronger reductions, approaching 99% in soot particle number emissions on the order of 10^{11} kg^{-1} have been demonstrated for lean-burn combustors operated with sustainable aviation fuels (SAFs) containing a high hydrogen content (Teoh et al., 2022a). However, these fuels do not reduce water vapour emissions.

The reduction in RFSW is consistently slightly more pronounced than the reduction in RFLW across all soot reduction scenarios. This is because shortwave scattering is highly sensitive to both the number and size of ice crystals, which in turn depend on the availability of soot particles as condensation nuclei. Fewer soot particles lead to fewer but larger ice crystals, which are less efficient at scattering incoming solar radiation, resulting in a stronger decrease in RFSW. In contrast, the reduction in RFLW is somewhat weaker, since longwave absorption and emission are less sensitive to particle size and more influenced by overall ice water content and contrail geometry. Consequently, RFnet (RFLW + RFSW) also decreases with soot reduction, although the longwave and shortwave contributions partially offset each other. The optical thickness (TAUCO) decreases even more strongly than the radiative fluxes in all cases. This is expected because TAUCO is directly related to the number concentration and projected area of ice crystals. While individual crystals grow larger when fewer nucleation sites are available, the total optical extinction remains dominated by the reduced number of particles. Moreover, increased sedimentation of larger crystals shortens contrail lifetime. The relative magnitude of changes, TAUCO > RFSW > RFLW > RFnet, remains stable throughout all examined soot reduction scenarios.

3.3. Reduction of water vapour emission

In this section we investigate the change in the mean values of RFLW, RFSW, RFnet and TAUCO (Table 1) over the full year 2019 with respect to our baseline scenario (0% soot reduction, 0% water vapour reduction) in Fig. 8 when water vapour emissions are reduced. The vertical axis indicate the percentage change of the simulated quantities relative to their corresponding baseline scenario (point (0,0)), while the horizontal axis represents the percentage reduction in water vapour emission. The water vapour adjustment is visualized in the range highlighted in light blue in Fig. 3.

Similar to Fig. 7, we observe that the mean percentage difference of the contrail radiative and optical properties decrease monotonically, here with increasing reduction of water vapour. For RFnet, a 50% reduction in water vapour results in about a 21% percentage decrease (for TAUCO 36%), while 90% reduction in water vapour leads to a RFnet decrease of approximately 90% (for TAUCO 95%). As before the curves decrease non-linearly and monotonically. In comparison to Fig. 7, the impact of a 90% reduction in water vapour on contrail properties is substantially more pronounced than that observed with soot reduction. This suggests that at such low levels of water vapour in the exhaust, contrails exist only in few regions with sufficiently cold temperatures to fulfil the SAC and become very thin, resulting in a considerably smaller overall radiative effect. The relative contribution of these effects, optical thinning or reduced occurrence, will be investigated in upcoming studies. Remember that this analysis represents average data collected in 2019 for the whole European domain. However, as shown in Fig. 4, both positive and negative RFnet values are predicted within the domain at this time step. To our knowledge, no further study about the effect of water vapour reduction in the aircraft exhaust is available in literature.

The relative ordering of reductions, with TAUCO decreasing most strongly, followed by RFSW, RFLW, and RFnet, is similar to the pattern observed for soot reduction in Section 3.3. However, the physical mechanism is different: reduced water vapour emission primarily affects contrail formation frequency and initial humidity conditions, leading to thinner and less frequent contrails overall.

3.4. Reduction of water vapour emission with reduced soot particle emission

In this section we first investigate the change in the mean values of RFLW, RFSW, RFnet and TAUCO (Table 1) over the full year 2019 with respect to a baseline scenario for 99% soot reduction in Fig. 9 when also water vapour emissions are reduced. The vertical axes indicate the percentage change of the simulated quantities relative to this baseline scenario (point (0,0)), while the horizontal axis represents the reduction in water vapour. The water vapour reduction analysis is referenced by the yellow highlighted parameter range in Fig. 3.

The results displayed in Fig. 9 are very similar to those in Fig. 8. In Fig. 9, the reference scenario (0,0) corresponds to 99% soot reduction without water vapour reduction, whereas Figs. 7 and 8 use 0% soot and 0% water vapour reduction as the baseline. As a result, the percentage

Table 2
Mean and standard deviation (W/m^2) of instantaneous net radiative forcing (RFnet) in 2019 over the European region, along with the total percentage difference of the mean RFnet relative to the baseline scenario (0% soot reduction, 0% water vapour reduction), for different reductions of soot and water vapour.

Soot reduction [%]	Water vapour reduction [%]	$RFnet_{mean}$ [W/m^2]	$RFnet_{std}$ [W/m^2]	$RFnet_{mean}$ difference [%]
0.0	0.0	0.21379	0.27053	−0.00
0.0	50.0	0.16956	0.20693	−20.69
0.0	90.0	0.02058	0.02969	−90.37
50.0	0.0	0.17157	0.21353	−19.75
50.0	50.0	0.13038	0.15760	−39.01
50.0	90.0	0.01457	0.02073	−93.18
90.0	0.0	0.08608	0.10480	−59.74
90.0	50.0	0.06041	0.07221	−71.74
90.0	90.0	0.00576	0.00809	−97.31
99.0	0.0	0.02517	0.03001	−88.23
99.0	50.0	0.01666	0.01972	−92.21
99.0	90.0	0.00143	0.00199	−99.33

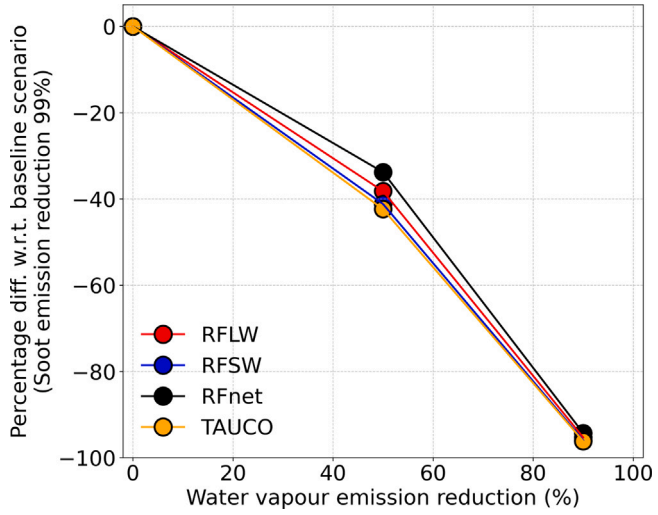

Fig. 9. Percentage difference of RFnet, RFSW, RFLW and TAUCO (see Table 1) w.r.t. the baseline scenario (99% soot emission reduction) vs. water vapour emission reduction (mean results for 2019).

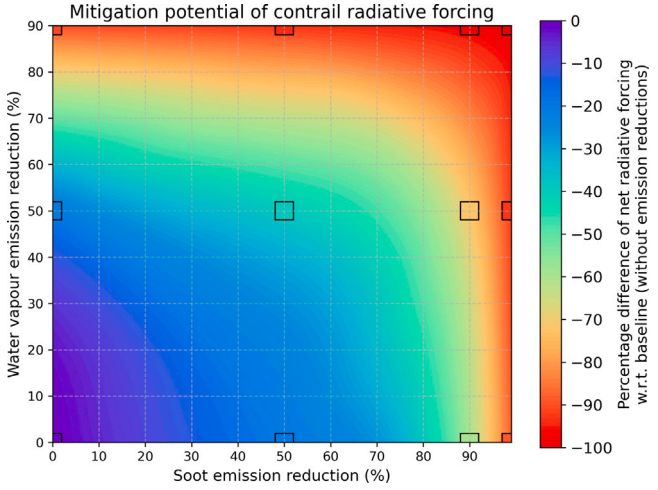

Fig. 10. Filled contour plot of the annual mean reduction in net radiative forcing (RFnet) as a function of soot and water vapour emission reductions. Colour shading indicates the interpolated percentage reduction relative to the baseline scenario without emission reductions. The plot is based on the 12 simulation cases listed in Table 2, which are marked by black squares. The response shows a smooth but nonlinear decrease in RFnet, with strongest mitigation occurring under combined soot and water vapour reductions.

changes in Fig. 9 are relative to a different baseline and should not be directly compared to those in Figs. 7 and 8.

This approach isolates the effect of water vapour reductions when soot emissions are already two orders of magnitude lower than in the reference situation. In this scenario with substantially lower soot content, a 50% reduction in water vapour results in a 34% reduction in RFnet (for TAUCO 42%), while a 90% reduction results in a 94% reduction in RFnet (for TAUCO 96%). This strong reduction in soot emissions by two orders of magnitude with a simultaneous reduction of 90% in water vapour emission leads to a strong attenuation of the radiative effects caused by contrails, which is also reflected in the absolute mean values for RFnet listed in Table 2, RFnet decreases from 0.214 W/m^2 to 0.001 W/m^2 which corresponds to an annual warming reduction over Europe down to 0.7% of the reference value.

The relative decrease of TAUCO, RFSW, RFLW, and RFnet again follows the same pattern as in Sections 3.2 and 3.3. This confirms that both emission reductions act complementarily, enhancing the total mitigation effect while preserving the characteristic order of percentage reductions.

Furthermore, we note that both shortwave (RFSW) and longwave (RFLW) radiative forcing exhibit nonlinear responses to soot and water vapour emission reductions, with steeper declines emerging beyond roughly one order of magnitude reduction (see Figs. 7–9). Consequently, both the dominant positive forcing and the rarer, weaker negative forcing (cooling) contrails (see Section 2.1, Figs. 4a, 8, 9, and the Supplementary Material) diminish more rapidly at higher reduction rates. Although occasional negative forcing events do occur, the overall trend is driven by the larger drop in positive forcing, because these warming contrails occur more frequently and with stronger effects, particularly under combined soot- and water-vapour reductions. Hence, our results confirm that simultaneous reductions in both soot and water vapour yield the most robust mitigation of contrail radiative forcing.

Finally, we summarize all RFnet results in Fig. 10, in particular for simultaneous reductions in soot and water vapour emissions. Based on the twelve discrete simulation cases listed in Table 2, each marked by a black square, the figure shows the interpolated annual mean reduction in RFnet as a function of both emission reductions. This offers a compact visual summary of the simulation results and helps identify effective combinations of mitigation strategies. Colour shading indicates the interpolated percentage reduction in RFnet relative to the baseline case (0% reduction in both soot and water vapour). The interpolation shows a continuous gradient and illustrates that RFnet is sensitive to both soot and water vapour emission reductions. Water vapour reduction by up to approx. 30% results first in a slower decrease in RFnet than for similar soot reductions. However, an RFnet reduction by 80% can be reached by water vapour reductions of ca. 80% or soot reductions larger than 90%. A similar mitigation can also be

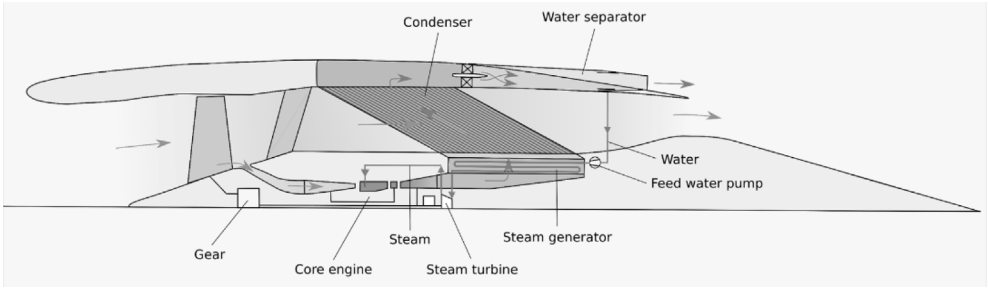

Fig. 11. Schematic of the Water-Enhanced Turbofan, originally published in Kaiser et al. (2022).

achieved by a combination of moderate reductions in both components. The contour plot reveals non-linear interactions, particularly at high emission reductions, where further decreases yield comparatively smaller additional mitigation. Moreover, contrail formation requires a minimum threshold of water vapour, independent of soot availability.

4. Low-soot, low water vapour engine concepts as the Water-Enhanced Turbofan

While the main focus of this study lies on idealized sensitivity analyses of contrail radiative forcing in response to soot and water vapour emission changes, this section provides an illustrative example of one conceptual propulsion architecture designed to reduce both emissions simultaneously.

The Water-Enhanced Turbofan (WET) concept aims to reduce soot, water vapour, NO_x, and CO_2 emissions simultaneously. It is currently at Technology Readiness Level (TRL) 2–3, with some technology bricks already experimentally demonstrated. It applies the Cheng Cycle, which combines the Joule/Brayton gas turbine cycle with the Clausius/Rankine steam cycle. A schematic drawing is shown in 11 (Kaiser et al., 2022; Schmitz et al., 2021; Ziegler et al., 2023).

Exhaust heat after the Low-Pressure Turbine (LPT, inside the "core engine" in the figure) is used in a steam generator to turn pressurized water into superheated steam. The steam is expanded in a steam turbine, which, together with the LPT, drives the fan. Steam is injected into the combustion chamber, increasing the heat capacity and mass flow of the working fluid.

This enhances the amount of specific work extracted in the expansion process. The incompressibility of water further contributes to this increase in specific power, since the compression of a purely liquid working fluid requires orders of magnitude less power than of a gas. Therefore, the core size can be reduced, which lowers the weight of the turbo components and increases the Bypass Ratio (BPR) for a given fan diameter.

To close the water cycle, water is extracted from the core exhaust flow. The water in the exhaust partially originates from the injection of steam into the combustion chamber and partially from combustion-generated water during the combustion of fuel (kerosene) with air. After passing the steam generator, the core exhaust is further cooled down below its dew point in the condenser, which is cooled with bypass air. Water droplets may nucleate on condensation nuclei such as aerosol and soot particles formed in the combustion process. The droplets can condense on surfaces and then be extracted with a water separator. The recovered water is then pressurized by a pump before entering the steam generator and could be stored onboard and released later in regions less prone to contrail formation, such as during descent or in drier atmospheric layers. However, no current engine design includes such a system, and practical implementation would require significant trade-offs, including added weight, increased system complexity, and certification challenges. More detailed information about the configuration and cycle is provided in Kaiser et al. (2022) and Schmitz et al. (2021).

The main advantages of the concept can be summarized as substantial improvements in all three climate-relevant effects (CO_2, NO_x, contrails). The practical challenges lie in integrating the required heat exchangers within the limited space available on aircraft and in ensuring reliable condensation performance under warm ambient conditions, such as during take-off.

Due to the extraction of heat from the core flow and the subsequent re-insertion into the cycle, the thermal efficiency is increased and the temperature of the exhaust gas is considerably reduced. Kaiser et al. (2022) and Ziegler et al. (2025) suggest that the exhaust conditions are less prone to fulfilling the SAC. In comparison to a turbofan with a similar technology level, the exhaust is drier, leading to a lower critical ambient temperature, T_c, below which contrails would form. This is achieved by condensing and extracting more water than is used for injection into the combustion chamber. The excess water can be stored and released in regions that are less sensitive to contrails.

The combustion soot particles are expected to be separated from the core exhaust flow together with the water droplets. This could decrease the number of condensation nuclei in the exhaust plume. Since not all of the water droplets can be extracted, and for operational weight considerations, a fraction of the condensed water could be emitted into the ambient air in a liquid state. Although these droplets contribute to contrail formation, their radiative forcing is expected to be small, especially when their size is considerably larger than that of typical combustion contrail particles. This effect remains to be quantified in future work.

The potential CO_2 savings associated with the WET configuration are based on thermodynamic cycle studies (Kaiser et al., 2022), not on demonstrator testing or operational data. The WET concept is aimed to recover up to 90% of the exhaust water vapour (Kaiser et al., 2022). While this value reflects an ideal design target, preliminary thermodynamic cycle studies suggest that partial recovery of around 50% may be achievable under certain conditions. Recovering larger fractions becomes increasingly difficult due to challenges in condensation efficiency and heat integration. For a typical WET concept engine design at the time of the study, water reductions of approximately 50% seemed thus achievable, whereas 90% represented design goals rather than demonstrated performance. These values are therefore used as idealized but technically plausible bounds in our emission reduction scenarios.

As of 2024, MTU has decided not to pursue further internal development of the concept beyond the research phase, citing limited fuel-saving potential under realistic design constraints. Still, the WET concept is an illustrative and inspiring example of a configuration that aims to reduce all four major contributors to aviation climate impact, namely CO_2, NO_x, water vapour, and soot particle numbers, within a single integrated engine configuration. The practical relevance of any such system would depend on future technological advances and economic feasibility. By the time large-scale deployment of new propulsion systems becomes possible, for instance in the 2040s or beyond, alternative technologies such as hydrogen combustion, electric propulsion, or operational mitigation strategies may also be viable.

For example, hydrogen combustion eliminates CO_2 and soot emissions. When combined with optimized navigational contrail avoidance, it may also help reduce the radiative effect of contrails. Nevertheless, hydrogen exhaust may contain significantly more water vapour than Jet-A, which could enhance contrail formation unless this is counteracted by specific mitigation strategies. However, exploring such scenarios is beyond the scope of this study.

While the WET concept is no longer under active development, it serves here as a conceptual archetype of a low-emission configuration for sensitivity testing. Our results do not depend on any specific technology being deployed.

5. Summary & conclusions

To investigate the contrail radiative effect of novel low-soot and low-water vapour engine concepts, we performed a set of sensitivity studies. These were conducted within the parameter range supported by the version of the CoCiP model developed for conventional turbofan engines with soot number emission indices between 10^{13} and 10^{16} particles per kilogramme of fuel. Volatile particles are considered only indirectly: aircraft engines in CoCiP are always supposed to produce at least 10^{13} contrail condensation nuclei.

As a first step, air traffic in one year over Europe is selected as a reference case and ice optical thickness as well as radiative effect of contrails are computed. In this manuscript, we utilize the meteorology and traffic data from 2019 as a baseline for our sensitivity studies. Therefore, while our results are specific to the meteorological conditions of 2019, they are not intended as a prediction for a future air traffic scenario with different climate conditions as they do not account for projected changes in climate variables such as tropopause height, background humidity, or atmospheric stability. Likewise, the analysis does not include future shifts in traffic density and fleet composition. Therefore, the RFnet values reported here should be interpreted as upper bounds under current conditions rather than as predictions for future decades.

In the second step, we simulate the impact of a reduction of soot emissions by 50%, 90% (i.e., one order of magnitude) and 99% (i.e., two orders of magnitude) on ice optical thickness and on the contrail instantaneous radiative forcing for the meteorological conditions in Europe in 2019. We apply the emission reduction equally to the entire fleet in 2019. A decrease in soot emissions by two orders of magnitude corresponds to reaching background particle concentrations for a current turbofan engine. The results show that the reduction of the radiative impact of contrail cirrus depends non-linearly on the soot particle number emission. The case of 50% less soot particles results in a reduction of RFnet by approximately 20%, while lowering the soot particle number to 90% yields a 60% reduction in contrail RFnet. These CoCiP simulations thus show a similar behaviour as global climate model (GCM) results from Bier and Burkhardt (2022) and Burkhardt et al. (2018), despite the different emission scenarios and computed radiative quantities, and the absence of interactive meteorological feedbacks in CoCiP. Note that CoCiP computes the *instantaneous top-of-atmosphere radiative forcing* over Europe, without accounting for rapid atmospheric adjustments. In contrast, the global climate models used in the cited studies report global *stratospherically adjusted radiative forcing*, which includes fast feedbacks, particularly in the stratosphere. While the absolute values are therefore not directly comparable, the relative trends with respect to soot emission reductions show consistent behaviour between both modelling approaches. A 99% reduction in soot particles enhances the reduction in contrail RFnet to 88%. Due to the reduction in the number of soot particles, the amount of available condensation nuclei and the number of ice crystals in contrails is expected to reduce. The emitted and ambient water vapour is distributed over fewer ice crystals such that reduced soot emissions result in fewer but larger ice particles. Larger particles have higher sedimentation rates. Therefore, the contrail lifetime and radiative effect are reduced.

In a third step, water vapour emissions in the exhaust are lowered by 50% and 90% while all other fuel and aircraft parameters have remained unchanged. This results in fewer water molecules and smaller contrail particles, which reduce the impact on the solar and thermal radiation budget and increase contrail dissipation rates. Moreover, the SAC is fulfilled in significantly fewer flight segments (i.e., only at lower ambient temperatures), leading to a decrease in overall contrail formation. In conjunction with these effects, RFnet decreases by 21% at 50% reduction in water vapour and by 90% at 90% reduction.

In a fourth step, soot number emission are lowered by 99% and held constant while water vapour is reduced in two steps as before. For such combinations we obtain a decrease in RFnet by 34% at 50% water vapour reduction and 94% at 90% reduction. In total, this corresponds to an 99% reduction in instantaneous radiative forcing when soot emissions are reduced by two orders of magnitude and water vapour emissions by one order of magnitude (see also Table 2). Lower soot emissions reduce the number of ice crystals, leading to fewer but larger particles, which enhances sedimentation and reduces contrail lifetime. Lower water vapour emissions decrease the occurrence of contrails by lowering plume humidity, thereby limiting the fulfilment of the SAC and leading to thinner contrails with reduced optical thickness. These processes modify contrail properties in different ways, resulting in a stronger overall reduction in contrail radiative forcing when both emissions are reduced simultaneously.

The comprehensive evaluation of single novel engine concepts was not the goal of this study. To this end, their emission characteristics and the physical processes involved should be first investigated with appropriate measurements at the ground and in-flight and the findings then integrated into CoCiP to obtain more detailed estimates of the contrail properties and radiative effects. For instance, for the contrails produced by the WET concept additional aspects would require further study, including improved engine efficiency, the emission of liquid water droplets, and the nucleation capacity of ambient aerosol or volatile particles formed in the exhaust, e.g., composed of sulfur or hydrocarbons (organics) (Yu et al., 1999, 2024) or from lubrication oil (Ungeheuer et al., 2022; Ponsonby et al., 2024). In particular, the latter process may reduce the mitigating effect of lowered soot emissions by providing alternative ice nucleation pathways (see discussion in Section 3.4). While WET is used here as an illustrative example, similar emission profiles might also result from alternative concepts such as hydrogen propulsion with exhaust treatment or advanced SAF blends.

The results from our parametric CoCiP-based study strongly suggest that low-soot and/or low-water vapour engines can substantially reduce the radiative forcing of contrail cirrus, particularly when soot and water vapour emissions are simultaneously reduced. These estimates should be interpreted with regard to the modelling assumptions outlined in Section 2.1. In particular, uncertainties arise from unrepresented alternative nucleation pathways and the absence of interactive microphysical feedbacks, which may affect the magnitude of the simulated mitigation effect. Despite these caveats, our results are consistent with broader modelling and observational literature indicating that reducing soot particle emissions leads to a substantial decline in contrail-induced positive radiative forcing (Bier and Burkhardt, 2022; Bier et al., 2017). Our results should be interpreted as the maximum mitigation potential that could be achieved through the adoption of low-soot and low-water vapour engines. Future studies based on observational evidence of the emission characteristics of specific technologies and the related physical processes in the aircraft plume and the atmosphere employing coupled climate models, high-resolution microphysical simulations and CoCiP will be essential for a more comprehensive evaluation of contrail lifecycles and global climate impact, particularly under near-zero soot conditions. Additionally, further investigation is required to assess the influence of secondary aerosol pathways, meteorological feedbacks,

and possible trade-offs with other emissions in a fully consistent framework. Within this broader context, the low-soot, low water vapour emission concept remains a promising approach for aviation climate mitigation.

While our simulation framework assumes uniform adoption of low-emission profiles across all flights, the RFnet maps shown in Figures 1s and 2s (Supplementary Material) reveal strong geographic heterogeneity indicating that significant mitigation could already be achieved through partial deployment on high-traffic routes. This highlights the importance of prioritizing early adoption in those areas with the highest contrail frequency and radiative forcing.

CRediT authorship contribution statement

Milenko Rubin-Zuzic: Writing – review & editing, Writing – original draft, Visualization, Software, Methodology, Investigation, Formal analysis, Data curation. **Luca Bugliaro:** Writing – review & editing, Writing – original draft, Visualization, Validation, Supervision, Methodology, Conceptualization. **Andreas Marsing:** Writing – review & editing, Writing – original draft, Visualization. **Ziming Wang:** Visualization, Software. **Christiane Voigt:** Writing – review & editing, Supervision, Methodology, Funding acquisition, Conceptualization. **Christopher Simson:** Writing – review & editing, Writing – original draft. **Sascha Kaiser:** Writing – review & editing, Writing – original draft. **Paul Ziegler:** Writing – review & editing, Writing – original draft.

Declaration of competing interest

Christopher Simson, Sascha Kaiser, and Paul Ziegler are employees of MTU Aero Engines AG. The remaining authors declare that they have no competing interests.

Acknowledgements

We thank Prof. Ulrich Schumann for providing us with the Fortran code of the CoCiP model, and for help and advice on various questions. We thank Liam Megill (DLR) and the anonymous reviewers for helpful comments on the manuscript. We acknowledge data contributed by EUMETSAT, ECMWF, EUROCONTROL, and NATS.

The research work associated with this publication has been supported by the German Federal Ministry for Economic Affairs and Climate Action (Bundesministerium für Wirtschaft und Klimaschutz, BMWK) under grant numbers 20M2110A and 20M2110B. The funding of the work through the 2nd call of the Federal Aviation Research Program VI (LuFo VI-2), grant project title 'DINA2030plus', is gratefully acknowledged.

Appendix A. Nomenclature

BADA3 Base of Aircraft Data 3

BPR Bypass-Ratio

CO_2 Carbon Dioxide

CoCiP Contrail Cirrus Prediction model

EASA European Union Aviation Safety Agency

ECMWF European Centre for Medium-Range Weather Forecasts

ERA5 ECMWF Fifth Generation Reanalysis

ERF Effective Radiative Forcing

EUROCONTROL European Organization for the Safety of Air Navigation

GCM General Circulation Model

IATA International Air Transport Association

ICAO International Civil Aviation Organization

IFS Integrated Forecasting System

ISSR Ice Supersaturated Region

LPT Low-Pressure Turbine

NO_x Sum of the Nitrogen Oxides NO and NO_2

RF Radiative Forcing

RFLW Longwave radiative forcing (from contrails)

RFSW Shortwave radiative forcing (from contrails)

RFnet Net radiative forcing: RFnet = RFLW + RFSW

RHi Relative Humidity with respect to ice

SAC Schmidt–Appleman Criterion

TAUCO Contrail optical depth (CoCiP output)

TRL Technology Readiness Level

vPM Volatile Particulate Matter

nvPM Non Volatile Particulate Matter

WET Water-Enhanced Turbofan

Appendix B. Supplementary data

Supplementary material related to this article can be found online at https://doi.org/10.1016/j.aeaoa.2025.100353.

Data availability

Data will be made available on request.

References

Appleman, H., 1953. The formation of exhaust contrails by jet aircraft. Bull. Am. Meteorol. Soc. 34, 14–20. http://dx.doi.org/10.1175/1520-0477-34.1.14.

Bier, A., Burkhardt, U., 2022. Impact of parametrizing microphysical processes in the jet and vortex phase on contrail cirrus properties and radiative forcing. J. Geophys. Res.: Atmospheres 127 (23), e2022JD036677. http://dx.doi.org/10.1029/2022JD036677, URL: https://agupubs.onlinelibrary.wiley.com/doi/abs/10.1029/2022JD036677.

Bier, A., Burkhardt, U., Bock, L., 2017. Synoptic control of contrail cirrus lifecycles and their modification due to reduced soot number emissions. J. Geophys. Res.: Atmospheres 122 (20), 11584–11603. http://dx.doi.org/10.1002/2017JD027011.

Bier, A., Unterstrasser, S., Zink, J., Hillenbrand, D., Jurkat-Witschas, T., Lottermoser, A., 2024. Contrail formation on ambient aerosol particles for aircraft with hydrogen combustion: a box model trajectory study. Atmospheric Chem. Phys. 24 (4), 2319–2344. http://dx.doi.org/10.5194/acp-24-2319-2024, URL: https://acp.copernicus.org/articles/24/2319/2024/.

Burkhardt, U., Bock, L., Bier, A., 2018. Mitigating the contrail cirrus climate impact by reducing aircraft soot number emissions. Npj Clim. Atmospheric Sci. 1 (37), 2397–3722. http://dx.doi.org/10.1038/s41612-018-0046-4.

Burkhardt, U., Kärcher, B., 2011. Global radiative forcing from contrail cirrus. Nat. Clim. Chang. 1, 54–58. http://dx.doi.org/10.1038/nclimate1068.

Dischl, R., Kaufmann, S., Voigt, C., 2022. Regional and seasonal dependence of the potential contrail cover and the potential contrail cirrus cover over Europe. Aerospace 9 (9), http://dx.doi.org/10.3390/aerospace9090485, URL: https://www.mdpi.com/2226-4310/9/9/485.

Dischl, R., Sauer, D., Voigt, C., Harlaß, T., Sakellariou, F., Märkl, R., Schumann, U., Scheibe, M., Kaufmann, S., Roiger, A., Dörnbrack, A., Renard, C., Gauthier, M., Swann, P., Madden, P., Luff, D., Johnson, M., Ahrens, D., Sallinen, R., Schripp, T., Eckel, G., Bauder, U., Le Clercq, P., 2024. Measurements of particle emissions of an A350-941 burning 100 % sustainable aviation fuels in cruise. Atmospheric Chem. Phys. 24 (19), 11255–11273. http://dx.doi.org/10.5194/acp-24-11255-2024, URL: https://acp.copernicus.org/articles/24/11255/2024/.

EASA, 2022. European aviation environmental report 2022. https://www.easa.europa.eu/en/light/topics/european-aviation-environmental-report-2022.

ECMWF, 2024. European centre for medium-range weather forecasts, L137 model level definitions. https://confluence.ecmwf.int/display/UDOC/L137+model+level+definitions.

Gierens, K., Matthes, S., Rohs, S., 2020. How well can persistent contrails be predicted? Aerospace 7 (12), http://dx.doi.org/10.3390/aerospace7120169, URL: https://www.mdpi.com/2226-4310/7/12/169.

IATA, 2025. Industry Statistics. https://www.iata.org/en/iata-repository/pressroom/fact-sheets/industry-statistics.

Kaiser, S., Schmitz, O., Ziegler, P., Klingels, H., 2022. The water-enhanced turbofan as enabler for climate-neutral aviation. Appl. Sci. 12 (23), http://dx.doi.org/10.3390/app122312431, URL: https://www.mdpi.com/2076-3417/12/23/12431.

Kärcher, B., 2018. Formation and radiative forcing of contrail cirrus. Nat. Commun. 9 (1824), http://dx.doi.org/10.1038/s41467-018-04068-0, 2041–1723.

Kärcher, B., Fahey, D.W., 1997. The role of sulfur emission in volatile particle formation in jet aircraft exhaust plumes. Geophys. Res. Lett. 24 (4), 389–392. http://dx.doi.org/10.1029/97GL00119.

Kärcher, B., Yu, F., 2009. Role of aircraft soot emissions in contrail formation. Geophys. Res. Lett. 36 (1), L01804. http://dx.doi.org/10.1029/2008GL036649.

Kleine, J., Voigt, C., Sauer, D., Schlager, H., Scheibe, M., Jurkat-Witschas, T., Kaufmann, S., Kärcher, B., Anderson, B.E., 2018. In situ observations of ice particle losses in a Young persistent contrail. Geophys. Res. Lett. 45 (24), 13,553–13,561. http://dx.doi.org/10.1029/2018GL079390, URL: https://agupubs.onlinelibrary.wiley.com/doi/abs/10.1029/2018GL079390.

Lee, D., Fahey, D., Skowron, A., Allen, M., Burkhardt, U., Chen, Q., Doherty, S., Freeman, S., Forster, P., Fuglestvedt, J., Gettelman, A., De León, R., Lim, L., Lund, M., Millar, R., Owen, B., Penner, J., Pitari, G., Prather, M., Sausen, R., Wilcox, L., 2021. The contribution of global aviation to anthropogenic climate forcing for 2000 to 2018. Atmos. Environ. 244, 117834. http://dx.doi.org/10.1016/j.atmosenv.2020.117834, URL: https://www.sciencedirect.com/science/article/pii/S1352231020305689.

Märkl, R.S., Voigt, C., Sauer, D., Dischl, R.K., Kaufmann, S., Harlaß, T., Hahn, V., Roiger, A., Weiß-Rehm, C., Burkhardt, U., Schumann, U., Marsing, A., Scheibe, M., Dörnbrack, A., Renard, C., Gauthier, M., Swann, P., Madden, P., Luff, D., Sallinen, R., Schripp, T., Le Clercq, P., 2024. Powering aircraft with 100 % sustainable aviation fuel reduces ice crystals in contrails. Atmospheric Chem. Phys. 24 (6), 3813–3837. http://dx.doi.org/10.5194/acp-24-3813-2024, URL: https://acp.copernicus.org/articles/24/3813/2024/.

Meerkötter, R., Schumann, U., Doelling, D.R., Minnis, P., Nakajima, T., Tsushima, Y., 1999. Radiative forcing by contrails. Meteorol. Atmos. Phys. 71 (1–2), 29–43. http://dx.doi.org/10.1007/s00585-999-1080-7, URL: https://link.springer.com/article/10.1007/s00585-999-1080-7.

Megill, L., Grewe, V., 2025. Investigating the limiting aircraft design-dependent and environmental factors of persistent contrail formation. Atmospheric Chem. Phys. 25, 4131–4149. http://dx.doi.org/10.5194/acp-25-4131-2025.

Petzold, A., Döpelheuer, A., Brock, C.A., Schröder, F., 1999. In situ observations and model calculations of black carbon emission by aircraft at cruise altitude. J. Geophys. Res.: Atmospheres 104 (D18), 22171–22181. http://dx.doi.org/10.1029/1999JD900460, URL: https://agupubs.onlinelibrary.wiley.com/doi/abs/10.1029/1999JD900460.

Platt, J.C., Shapiro, M.L., Engberg, Z., McCloskey, K., Geraedts, S., Sankar, T., Stettler, M.E.J., Teoh, R., Schumann, U., Rohs, S., 2024. The effect of uncertainty in humidity and model parameters on the prediction of contrail energy forcing. Environ. Res. Commun. 6 (9), 095015. http://dx.doi.org/10.1088/2515-7620/ad6ee5, URL: https://iopscience.iop.org/article/10.1088/2515-7620/ad6ee5.

Ponsonby, J., King, L., Murray, B.J., Stettler, M.E.J., 2024. Jet aircraft lubrication oil droplets as contrail ice-forming particles. Atmospheric Chem. Phys. 24 (3), 2045–2058. http://dx.doi.org/10.5194/acp-24-2045-2024, URL: https://acp.copernicus.org/articles/24/2045/2024/.

Schmitz, O., Klingels, H., Kufner, P., 2021. Aero engine concepts beyond 2030: Part 1-the steam injecting and recovering aero engine. J. Eng. Gas Turbines Power 143 (2), 021001. http://dx.doi.org/10.1115/1.4048985.

Schumann, U., 1996. On conditions for contrail formation from aircraft exhausts. Meteorol. Z. 5, 4–23. http://dx.doi.org/10.1127/metz/5/1996/4.

Schumann, U., 2012. A contrail cirrus prediction model. Geosci. Model. Dev. 5 (3), 543–580. http://dx.doi.org/10.5194/gmd-5-543-2012.

Schumann, U., Bugliaro, L., Dörnbrack, A., Baumann, R., Voigt, C., 2021a. Aviation contrail cirrus and radiative forcing over Europe during 6 months of COVID-19. Geophys. Res. Lett. 48 (8), e2021GL092771. http://dx.doi.org/10.1029/2021GL092771, URL: https://agupubs.onlinelibrary.wiley.com/doi/abs/10.1029/2021GL092771, e2021GL092771 2021GL092771.

Schumann, U., Graf, K., 2013. Aviation-induced cirrus and radiation changes at diurnal timescales. J. Geophys. Res.: Atmospheres 118 (5), 2404–2421. http://dx.doi.org/10.1002/jgrd.50184, URL: https://agupubs.onlinelibrary.wiley.com/doi/10.1002/jgrd.50184.

Schumann, U., Heymsfield, A.J., 2017. On the life cycle of individual contrails and contrail cirrus. Meteorol. Monogr. 58, 3.1 – 3.24. http://dx.doi.org/10.1175/AMSMONOGRAPHS-D-16-0005.1, URL: https://journals.ametsoc.org/view/journals/amsm/58/1/amsmonographs-d-16-0005.1.xml.

Schumann, U., Penner, J.E., Chen, Y., Zhou, C., Graf, K., 2015. Dehydration effects from contrails in a coupled contrail–climate model. Atmospheric Chem. Phys. 15 (19), 11179–11199. http://dx.doi.org/10.5194/acp-15-11179-2015, URL: https://acp.copernicus.org/articles/15/11179/2015/.

Schumann, U., Poll, I., Teoh, R., Koelle, R., Spinielli, E., Molloy, J., Koudis, G.S., Baumann, R., Bugliaro, L., Stettler, M., Voigt, C., 2021b. Air traffic and contrail changes over europe during COVID-19: a model study. Atmospheric Chem. Phys. 21 (10), 7429–7450. http://dx.doi.org/10.5194/acp-21-7429-2021, URL: https://acp.copernicus.org/articles/21/7429/2021/.

Schumann, U., Ström, J., Busen, R., Baumann, R., Gierens, K., Krautstrunk, M., Schröder, F.P., Stingl, J., 1996. In situ observations of particles in jet aircraft exhausts and contrails for different sulfur-containing fuels. J. Geophys. Res.: Atmospheres 101 (D3), 6853–6869. http://dx.doi.org/10.1029/95JD03405, URL: https://agupubs.onlinelibrary.wiley.com/doi/abs/10.1029/95JD03405.

Teoh, R., Engberg, Z., Shapiro, M., Dray, L., Stettler, M.E.J., 2024. The high-resolution global aviation emissions inventory based on ADS-B (GAIA) for 2019–2021. Atmospheric Chem. Phys. 24 (1), 725–744. http://dx.doi.org/10.5194/acp-24-725-2024, URL: https://acp.copernicus.org/articles/24/725/2024/.

Teoh, R., Schumann, U., Gryspeerdt, E., Shapiro, M., Molloy, J., Koudis, G., Voigt, C., Stettler, M.E.J., 2022a. Aviation contrail climate effects in the North Atlantic from 2016 to 2021. Atmospheric Chem. Phys. 22 (16), 10919–10935. http://dx.doi.org/10.5194/acp-22-10919-2022, URL: https://acp.copernicus.org/articles/22/10919/2022/.

Teoh, R., Schumann, U., Voigt, C., Schripp, T., Shapiro, M., Engberg, Z., Molloy, J., Koudis, G., Stettler, M.E.J., 2022b. Targeted use of sustainable aviation fuel to maximize climate benefits. Environ. Sci. Technol. 56 (23), 17246–17255. http://dx.doi.org/10.1021/acs.est.2c05781, PMID: 36394538.

Timko, M.T., Onasch, T.B., Northway, M.J., Jayne, J.T., Canagaratna, M.R., Herndon, S.C., Wood, E.C., Miake-Lye, R.C., Knighton, W.B., 2010. Gas turbine engine emissions—Part II: Chemical properties of particulate matter. J. Eng. Gas Turbines Power 132 (6), 061505. http://dx.doi.org/10.1115/1.4000132.

Ungeheuer, F., Caudillo, L., Ditas, F., Simon, M., van Pinxteren, D., Kiliç, D., Rose, D., Jacobi, S., Kürten, A., Curtius, J., Vogel, A.L., 2022. Nucleation of jet engine oil vapours is a large source of aviation-related ultrafine particles. Commun. Earth & Environ. 3 (319), 2662–4435. http://dx.doi.org/10.1038/s43247-022-00653-w.

Unterstrasser, S., 2014. Large-eddy simulation study of contrail microphysics and geometry during the vortex phase and consequences on contrail-to-cirrus transition. J. Geophys. Res.: Atmospheres 119 (12), 7537–7555. http://dx.doi.org/10.1002/2013JD021418, URL: https://agupubs.onlinelibrary.wiley.com/doi/abs/10.1002/2013JD021418.

Unterstrasser, S., 2016. Properties of young contrails – a parametrisation based on large-eddy simulations. Atmospheric Chem. Phys. 16 (4), 2059–2082. http://dx.doi.org/10.5194/acp-16-2059-2016, URL: https://acp.copernicus.org/articles/16/2059/2016/.

Unterstrasser, S., Gierens, K., 2010. Numerical simulations of contrail-to-cirrus transition – part 2: Impact of initial ice crystal number, radiation, stratification, secondary nucleation and layer depth. Atmospheric Chem. Phys. 10 (4), 2037–2051. http://dx.doi.org/10.5194/acp-10-2037-2010, URL: https://acp.copernicus.org/articles/10/2037/2010/.

Verma, P., Burkhardt, U., 2022. Contrail formation within cirrus: ICON-LEM simulations of the impact of cirrus cloud properties on contrail formation. Atmospheric Chem. Phys. 22 (13), 8819–8842. http://dx.doi.org/10.5194/acp-22-8819-2022, URL: https://acp.copernicus.org/articles/22/8819/2022/.

Wang, Z., Bugliaro, L., Gierens, K., Hegglin, M.I., Rohs, S., Petzold, A., Kaufmann, S., Voigt, C., 2025. Machine learning for improvement of upper-tropospheric relative humidity in ERA5 weather model data. Atmospheric Chem. Phys. 25 (5), 2845–2861. http://dx.doi.org/10.5194/acp-25-2845-2025, URL: https://acp.copernicus.org/articles/25/2845/2025/.

Wolf, K., Bellouin, N., Boucher, O., Rohs, S., Li, Y., 2025. Correction of ERA5 temperature and relative humidity biases by bivariate quantile mapping for contrail formation analysis. Atmospheric Chem. Phys. 25 (1), 157–181. http://dx.doi.org/10.5194/acp-25-157-2025.

Yu, F., Kärcher, B., Anderson, B.E., 2024. Revisiting contrail ice formation: Impact of primary soot particle sizes and contribution of volatile particles. Environ. Sci. Technol. 58 (40), 17650–17660. http://dx.doi.org/10.1021/acs.est.4c04340, PMID: 39323293.

Yu, F., Turco, R.P., Kärcher, B., 1999. The possible role of organics in the formation and evolution of ultrafine aircraft particles. J. Geophys. Res.: Atmospheres 104 (D4), 4079–4087. http://dx.doi.org/10.1029/1998JD200062, URL: https://agupubs.onlinelibrary.wiley.com/doi/abs/10.1029/1998JD200062.

Ziegler, P., Kaiser, S., Gümmer, V., 2023. Parametric cycle studies of the water-enhanced turbofan concept. In: Proceedings of ASME Turbo Expo 2023: Turbomachinery Technical Conference and Exposition, June 26–30, 2023. In: Turbo Expo: Power for Land, Sea, and Air, vol. 5: Cycle Innovations, Boston, Massachusetts, USA, V005T06A001. http://dx.doi.org/10.1115/GT2023-100529, URL: https://doi.org/10.1115/GT2023-100529.

Ziegler, P., Simson, C., Arzberger, T., Woitalka, A., Nöske, F., Kaiser, S., Gümmer, V., 2025. Water-enhanced turbofan condenser sizing considering configuration and operating conditions. The Aeronautical Journal 129, 1494–1514. http://dx.doi.org/10.1017/aer.2024.158, URL: https://www.cambridge.org/core/journals/aeronautical-journal/article/abs/waterenhanced-turbofan-condenser-sizing-considering-configuration-and-operating-conditions/65EF0BECAB754ED66E333BF1D7B08975.